ARTICLES
PUBLISHED ONLINE: 11 MAY 2014 | DOI: 10.1038/NPHOTON.2014.85
nature photonics

Terahertz laser frequency combs

David Burghoff[1]*, Tsung-Yu Kao[1], Ningren Han[1], Chun Wang Ivan Chan[1], Xiaowei Cai[1], Yang Yang[1], Darren J. Hayton[2], Jian-Rong Gao[2,3], John L. Reno[4] and Qing Hu[1]

Terahertz light can be used to identify numerous complex molecules, but has traditionally remained unexploited due to the lack of powerful broadband sources. Pulsed lasers can be used to generate broadband radiation, but such sources are bulky and produce only microwatts of average power. Conversely, although terahertz quantum cascade lasers are compact semiconductor sources of high-power terahertz radiation, their narrowband emission makes them unsuitable for complex spectroscopy. In this work, we demonstrate frequency combs based on terahertz quantum cascade lasers, which combine the high power of lasers with the broadband capabilities of pulsed sources. By fully exploiting the quantum-mechanically broadened gain spectrum available to these lasers, we can generate 5 mW of terahertz power spread across 70 laser lines. This radiation is sufficiently powerful to be detected by Schottky-diode mixers, and will lead to compact terahertz spectrometers.

Optical frequency combs[1] have revolutionized high-precision metrology and spectroscopy[2]. At long-wavelength terahertz frequencies, combs generated by pulsed lasers[3] have proven to be useful sources of radiation for detecting molecular fingerprints, because many molecules have strong rotational and vibrational resonances in the terahertz regime[4,5]. However, these sources have difficulty achieving powers of more than a few microwatts, are typically detected coherently, and are bulky and involve expensive mode-locked lasers. Terahertz quantum cascade lasers[6] (THz QCLs), on the other hand, are powerful compact sources of such radiation and are capable of generating watt-level power output[7]. If they could be made to generate the uniformly spaced lines of a frequency comb, they would be ideal candidates for making compact spectrometers.

There are many ways to generate optical frequency combs, including intracavity phase modulation[8], pumping microresonators with high-intensity radiation[9], downconversion of a higher-frequency comb[10] and upconversion of a lower-frequency source[11,12]. However, the most powerful sources of frequency combs are generally mode-locked lasers, which in the time domain create a train of pulses and in the frequency domain create uniformly spaced lines. Mode-locked lasers can be classified into two varieties: actively mode-locked lasers, in which pulses are generated by an external modulation of the laser gain at the round-trip frequency, and passively mode-locked lasers, in which pulses generate their own modulation with the aid of saturable absorbers. Unfortunately, because external modulation is never as short as the pulse itself, actively mode-locked lasers cannot produce pulses as short as passively mode-locked lasers[13]. In the frequency domain, the spectral bandwidths of actively mode-locked lasers are therefore much narrower than those of passive ones.

In QCLs, mode-locking is difficult to achieve as the picosecond gain recovery time of the laser prevents stable pulse formation[14]. Although active mode-locking of mid-infrared QCLs[15] and THz QCLs[16] has been achieved, they were unable to exploit the full gain bandwidth available to the laser. On the other hand, recent work has demonstrated that when the group velocity dispersion (GVD) of a mid-infrared QCL is made sufficiently low by using a broadband heterogeneous gain medium, such devices can passively form frequency combs based on four-wave mixing[17]. Although this mechanism does not produce time-domain pulses with high peak intensities, the frequency comb produced is suitable for linear applications such as dual-comb spectroscopy[18,19] and optical coherence tomography[20]. Using this approach, Hugi *et al.*[17] increased the bandwidth of mid-infrared QCL combs from the 15 cm^{-1} achieved using active mode-locking to over 60 cm^{-1} (at 7 μm). However, a straightforward implementation of this approach is unlikely to work at terahertz frequencies, because terahertz electromagnetic waves strongly couple with the crystalline lattice and are thus orders of magnitude more dispersive than mid-infrared waves. Figure 1a shows the calculated GVD of GaAs at 40 K. At 3.5 THz, the GVD is 87,400 $fs^2\ mm^{-1}$, which is 250 times greater than the GVD at 7 μm (320 $fs^2\ mm^{-1}$). Simply using a broadband gain medium is not sufficient to overcome the dispersion of the material itself and permit comb formation.

To overcome this problem, we integrated dispersion compensation into our waveguides to deliberately cancel the cavity dispersion. The basic idea, illustrated in Fig. 1b, is that a chirped corrugation is etched into the facet of the laser, the period of which tapers from short to long as its amplitude increases. Long-wavelength waves (which have higher group velocities) travel to the end of the cavity before reflecting, while short-wavelength waves reflect earlier, thereby compensating dispersion. Essentially, this corrugation mimics the double-chirped mirrors used to generate octave-spanning spectra in the near-infrared and visible range[21]. To design such compensators, an accurate measurement of the dispersion of a real laser waveguide is essential. For this, terahertz time-domain spectroscopy[22] (THz TDS) was performed on single-section metal–metal waveguide lasers, using the biased QCL itself as a generator of time-domain pulses. Although this method is less accurate than two-section techniques for measuring laser gain[23–25], it permits a cleaner measurement of the round-trip phase because the terahertz pulse does not encounter gaps that could distort the transmitted pulse. The inset of Fig. 1a shows the phase acquired by a

[1]Department of Electrical Engineering and Computer Science, Research Laboratory of Electronics, Massachusetts Institute of Technology, Cambridge, Massachusetts 02139, USA, [2]SRON Netherlands Institute for Space Research, 9747 AD, Groningen, The Netherlands, [3]Kavli Institute of NanoScience, Delft University of Technology, Lorentzweg 1, 2628 CJ Delft, The Netherlands, [4]Center for Integrated Nanotechnology, Sandia National Laboratories, Albuquerque, New Mexico 87123, USA. *e-mail: burghoff@mit.edu

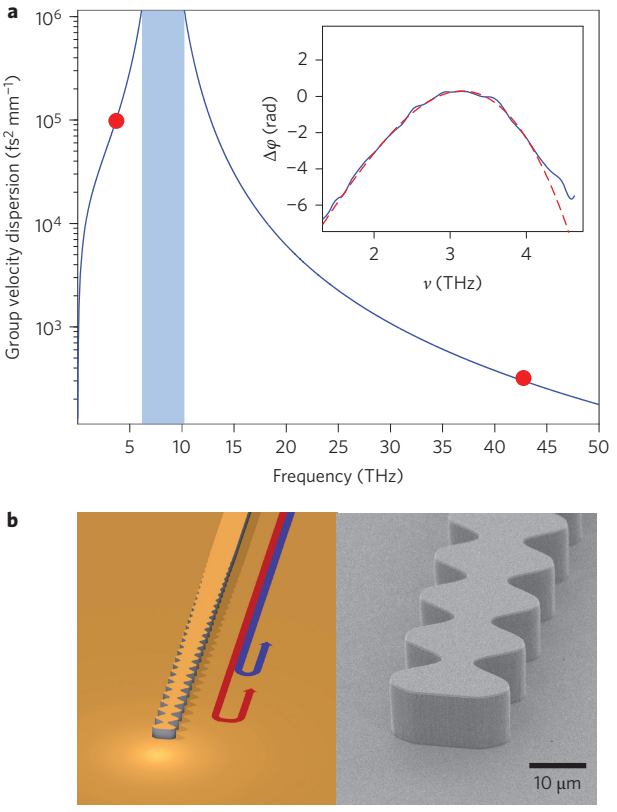

Figure 1 | GVD of laser gain medium. a, Calculated GVD of GaAs at 40 K, defined here as $D_2 \equiv \partial_\omega(1/v_g)$. The marked frequencies are 3.5 THz and 42 THz. Inset: phase acquired by a time-domain terahertz pulse after travelling through a 775 μm QCL twice, with a parabolic fit. **b**, Schematic of the integrated dispersion compensation scheme used. The longer-wavelength wave travels further before it reflects, while the shorter-wavelength wave reflects earlier, resulting in a shorter effective cavity.

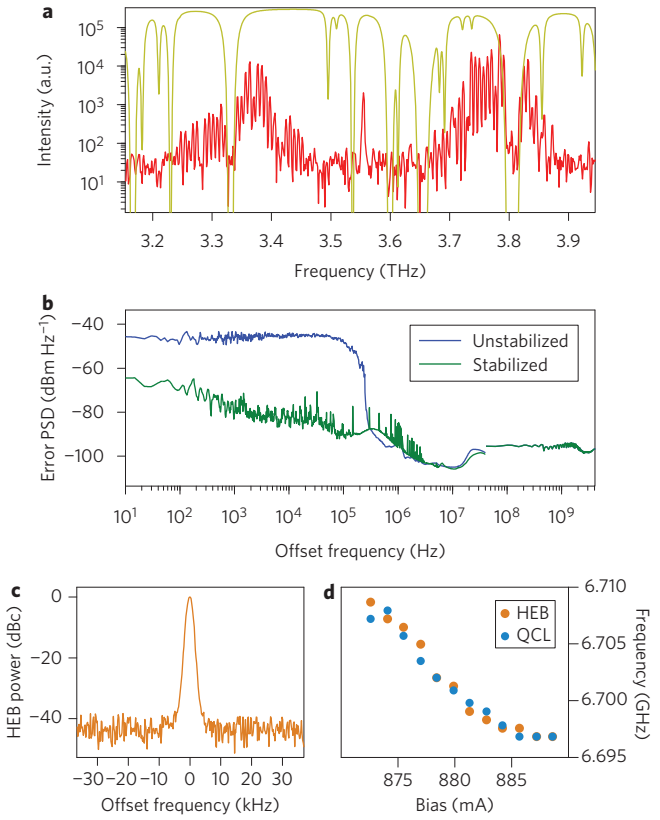

Figure 2 | Continuous-wave spectrum and beat notes. a, Spectrum of a THz QCL comb biased to 0.9 A at a temperature of 50 K. The device is 20 μm wide, 5 mm long and emits 4.7 mW at 45 K. Atmospheric absorption is shown in yellow. **b**, QCL-generated beat notes offset relative to 6.82 GHz, shown with the environmental fluctuations stabilized and unstabilized. (The spectra are discontinuous at 40 MHz because the signal below 40 MHz was measured by downconverting and sampling, while the signal above was measured with a spectrum analyser.) **c**, HEB-detected beat-note offset relative to 6.80 GHz, stabilized. The linewidth of 1.53 kHz is limited by the instrument resolution. **d**, Bias dependence of the beat-note frequency measured by the QCL and by the HEB. A repetition rate tuning of 12 MHz is possible, giving a total frequency shift of 6.80 GHz at 3.8 THz, approximately the mode spacing.

pulse after travelling through a 775-μm-long laser twice; the highly nonlinear phase–frequency relation indicates a GVD of $D_2 = 111{,}000\ \mathrm{fs^2\ mm^{-1}}$, which is substantially higher than what would be expected from GaAs alone. To account for uncertainties in the measurement and in device fabrication, seven different compensators were designed, which compensated the measured D_2 adjusted by 0%, ±6.6%, ±13.3% and ±20%. Details of the design parameters can be found in Supplementary Fig. 1.

Figure 2a shows the broad terahertz spectrum generated by a correctly GVD-compensated 5-mm-long QCL with a hyperhemispherical lens attached[26]. Because the gain medium—a homogeneous four-well resonant phonon design—has a strong injector anticrossing, the gain medium has two peaks, one near 3.3 THz and one near 3.8 THz (ref. 27). However, only the design overcompensated by +13.3% produces such a broad spectrum; the rest lase at only a few modes, indicating that it is essential to correctly compensate GVD for possible comb formation.

An interesting side effect of the broadband terahertz generation is that this same design—and only this design (Supplementary Fig. 1c)—generates a strong RF beat note at the round-trip frequency of the laser (~6.8 GHz) when d.c.-biased. Without taking into account RF losses from the bond wire, as much as −33 dBm of power has been observed leaking out of the 5 mm QCLs, as measured using a bias-tee. Although similar beat notes have previously been observed on the bias lines of metal–metal waveguides[28], at −65 dBm they were three orders of magnitude weaker. This strong RF signal implies that the beat notes generated from all the pairs in the spectra are adding up coherently. Figure 2b shows the RF beat note emanating from such a laser, offset relative to a local oscillator at its repetition rate. Because the devices are mounted in a pulsed-tube cryocooler, mechanical vibrations cause the optical feedback to be unstable and impart low-frequency fluctuations on the beat note. By slowly applying a sub-milliamp modulation to the bias of the laser (Supplementary Fig. 2), we remove 99.92% of its free-running phase noise and stabilize its output. No major sidebands are visible other than the one at 350 kHz created by the phase-locked loop.

We now show that the beat-note-producing devices indeed possess the uniformly spaced lines of a frequency comb. A straightforward way to test this is to shine the laser light onto a fast detector and to examine the resulting optical beating between all the laser modes. If only one narrow beat note were observed, that would indicate that all of the detected modes were evenly spaced. Conversely, a non-comb would have multiple beat notes; for example, two frequencies separated by 500 GHz would have mode spacings differing by hundreds of megahertz. For this measurement we used a superconducting NbN hot-electron bolometer mixer (HEB), because of its extreme sensitivity[29] and response beyond 7 GHz (ref. 30). Figure 2c shows a stabilized beat note measured

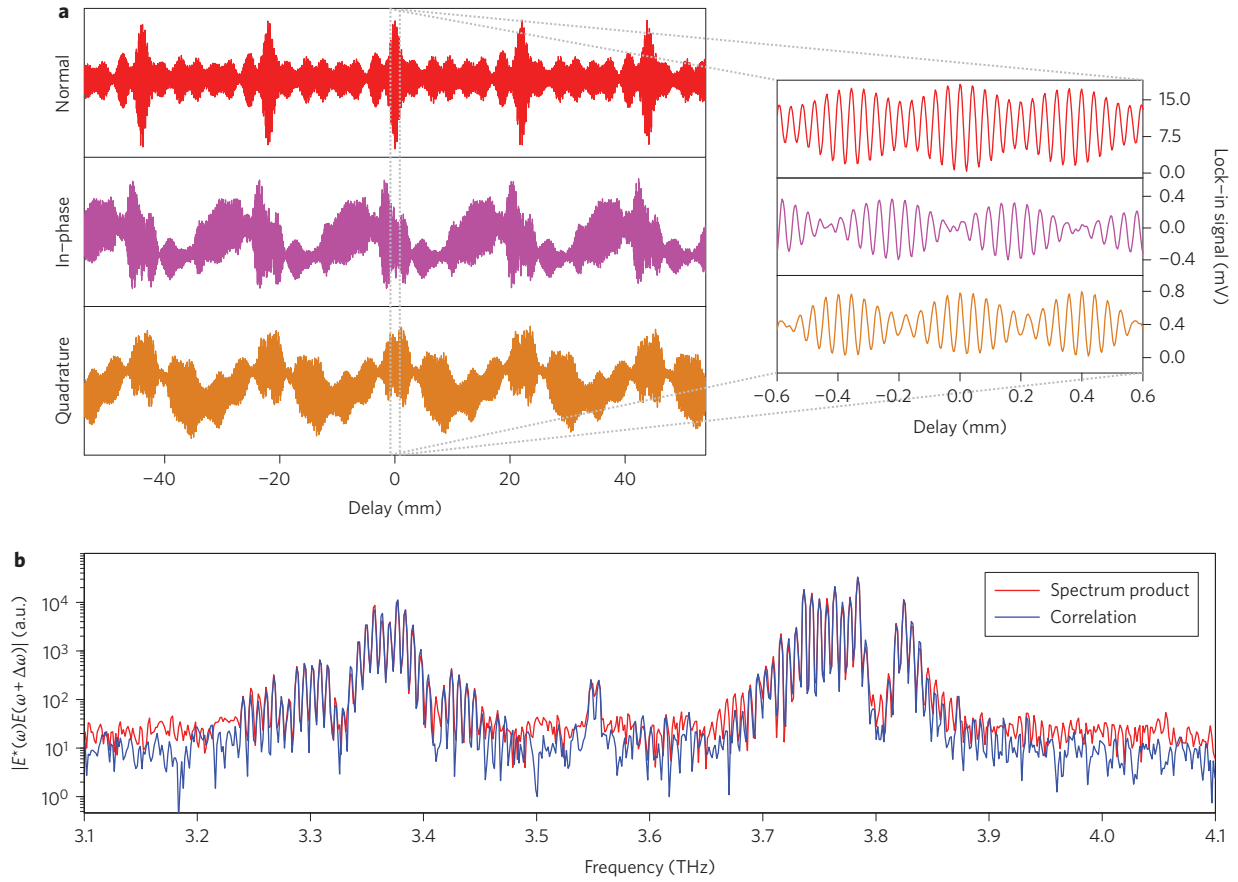

Figure 3 | Results of SWIFT measurement. a, Normal interferogram and homodyne interferograms, as measured by the HEB. The normal interferogram represents a d.c. measurement, while the homodyne interferogram represents an RF measurement. The QCL is biased to 0.9 A and is at 50 K. Inset: zoomed-in view near the zero-path delay. **b**, Blue line: SWIFT correlation spectrum (calculated from homodyne interferograms). Red line: spectrum product (calculated from normal interferogram). Even though they are fundamentally different measurements, their excellent agreement indicates that most of the spectral power is in the frequency comb.

with the HEB, and Fig. 2d compares its bias dependence to the beat note measured from the QCL using a bias-tee. The close agreement between the two frequencies shows that the beat note from the QCL well characterizes the beat note from the HEB. In addition, the narrow linewidth of the stabilized HEB beat note (under 2 Hz; Supplementary Fig. 2b) implies that the mutual phase coherence between all the detected modes persists for over 1×10^9 round trips through the laser cavity[31].

Of course, the existence of a narrow beat note on a fast detector and a broad spectrum does not prove that all of the modes observed in the spectrum are actually contributing to that beat note; it might be the case that a strong pair dominates the beat note. We stress that conventional spectroscopic techniques like Fourier-transform spectroscopy (FTS) cannot be used to determine the presence of a comb, because their resolution is limited by the physical travel of a mechanical delay element and can only measure spectra to a resolution of ~1 GHz. To truly show that all the modes in the spectrum are uniformly spaced, we use an interferometric technique that functions by examining the components of the RF beat note as a function of the delay of a Michelson interferometer. In this scheme, we lock the repetition rate of the QCL to a synthesizer at frequency $\Delta\omega$ and use that as a local oscillator for the homodyne detection of two signals, an in-phase signal ($S_I(\tau)$) and an in-quadrature signal ($S_Q(\tau)$). (Previous work has examined only the intensity of the RF beat note; here we also record its phase[17].) The advantage of this technique is that the Fourier transforms of the homodyne interferograms can be used to directly infer the correlation of the electric field of a light source with a frequency-shifted version of itself, by the relation

$$\langle E^*(\omega)E(\omega \pm \Delta\omega)\rangle = \frac{1}{2}(S_I(\omega) \mp iS_Q(\omega)) \equiv X_{\pm}(\omega)$$

where $E(\omega)$ is the electric field of the source, angle brackets represent an average over laboratory timescales (in seconds) and a convolution with the instrument's apodization function, $S_I(\omega)$ and $S_Q(\omega)$ are the Fourier transforms of the measured homodyne interferograms, and $X_{\pm}(\omega)$ are referred to as 'correlations'. We call this shifted wave interference Fourier-transform spectroscopy, or SWIFT spectroscopy for short. A normal Fourier-transform spectrum measures the d.c. component of the optical power through an interferometer, whereas a SWIFT spectrum measures its fast-varying components. (For more details, see Supplementary section 'SWIFT spectroscopy analysis'.)

There are some key differences between conventional FTS and SWIFT spectroscopy. For incoherent light sources, the SWIFT spectrum vanishes altogether, because the long-term phase incoherence between $E(\omega)$ and $E(\omega+\Delta\omega)$ causes their product to integrate to zero over laboratory timescales. Similarly, for a source consisting of two laser lines separated by $\omega_1 - \omega_2 \neq \Delta\omega$, the SWIFT spectrum is zero if $\omega_1 - \omega_2 - \Delta\omega$ is larger than the integration bandwidth (Hz). In contrast, one may use a normal Fourier-transform spectrum to define a 'spectrum product' as $X_{sp}(\omega) \equiv \sqrt{\langle|E(\omega)|^2\rangle\langle|E(\omega+\Delta\omega)|^2\rangle}$ and while this product is superficially

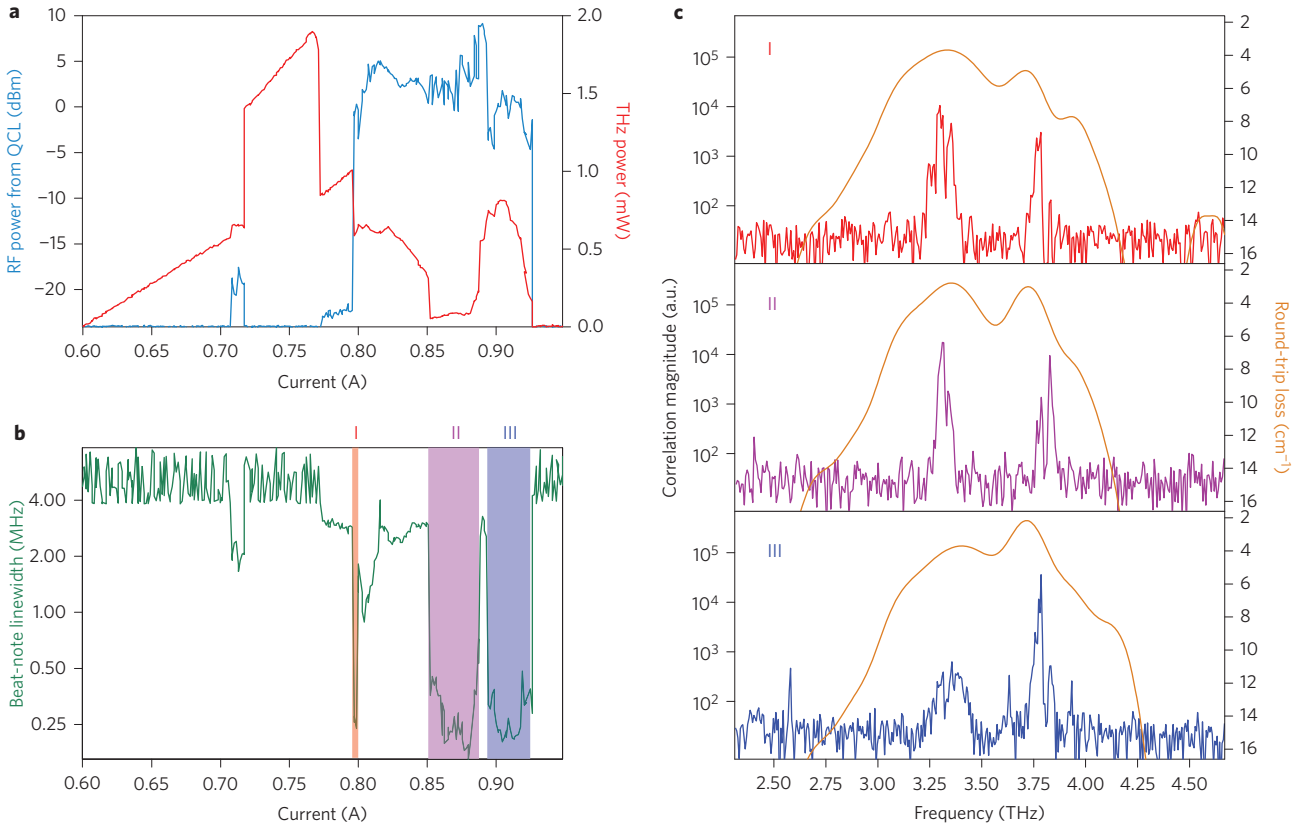

Figure 4 | Bias dependence of beat-note and SWIFT spectra. a, RF power measured from a bias-tee (amplified by 66 dB, with wiring losses of 20 dB) and terahertz power (calibrated) emitted by the QCL as a function of bias at 50 K, over the dynamic range of lasing operation. **b**, Linewidth of the RF signal emitted from the QCL as a function of bias, as measured with a spectrum analyser. (The linewidth metric used here is standard deviation.) The regions of stable comb formation are shaded and denoted I, II and III. **c**, SWIFT correlation spectra (measured with the HEB) and gain spectra (measured with THz TDS) corresponding to each of the three regions.

similar to $|X_+(\omega)|$, it will be non-zero as long as $\omega_1 - \omega_2 - \Delta\omega$ is within the spectrometer's resolution (GHz). We can therefore compare $|X_+(\omega)|$ and $X_{sp}(\omega)$ to reveal how comb-like a given laser spectrum is.

Figure 3a shows the SWIFT interferograms measured from a device biased to 0.9 A, together with a normal interferogram obtained at the same bias. Note that, although all three interferograms are nearly periodic with a spacing determined by the repetition rate of the laser, the SWIFT interferograms have non-zero phase and as a result are asymmetric about the zero path difference. In Fig. 3b we compare the correlation magnitude, calculated using SWIFT spectroscopy and the spectrum product, calculated using FTS. Their excellent agreement shows that essentially all of the laser's lines are separated by the repetition rate and we can truly call this a frequency comb. The correlation measurement shows approximately 70 comb lines above the noise floor, which span a total range of almost 500 GHz.

To see how the bias affects comb operation, we plot in Fig. 4a the optical and RF power generated by a QCL comb versus its bias in the range over which the device lases. At the onset of strong RF emission, there is a drop in total optical power that corresponds to the onset of comb formation. Similarly, Fig. 4b shows the linewidth of the QCL's RF emission versus bias. Not all biases within the range of strong RF emission actually form frequency combs, as there are certain biases at which the beat-note linewidth abruptly increases to several megahertz. Nonetheless, there are three distinct regions in which the beat-note linewidth is narrow and a stable comb is formed, denoted by regions I, II and III. To see whether we can actually exploit the full gain bandwidth at a given laser bias, we compared the SWIFT spectra obtained in the three regions of comb formation with the gain spectra measured by terahertz time-domain spectroscopy, and plotted the result in Fig. 4c. In region I, the lower-frequency lobe experiences more gain and, as a result, the corresponding portion of the correlation spectrum dominates. In region II, the two lobes of the gain and correlation spectra are approximately equal in strength. In region III, the higher-frequency lobe is stronger and lases more strongly. This result demonstrates the effectiveness of the dispersion compensation technique, because it shows that frequency combs can be formed under various conditions with different gain profiles.

Finally, we beat our comb with a single-mode distributed-feedback (DFB) laser to investigate the absolute linewidth of each comb line. For this measurement, we shine the DFB laser directly into the facet of our comb laser and examine the heterodyne beating that is generated by the intracavity mixing[32] of the DFB laser and the comb laser. Although fast detectors like HEBs or Schottky mixers can be used to measure similar properties, this measurement also demonstrates one of the salient features of our comb: the ability to detect the frequency of terahertz lasers without any additional components (modulo the repetition rate). Figure 5a shows the spectra of the two lasers involved: a single-mode DFB laser at ~3.85 THz and the SWIFT spectrum of a comb biased near 0.9 A. Figure 5b shows the beat notes generated by our devices over a large frequency span. At a given bias, there are two lines present below the repetition rate, corresponding to beating of the DFB laser with the two nearest adjacent comb lines. Their frequencies therefore add up to the repetition rate of the comb. When the frequency of the DFB is shifted by shifting its

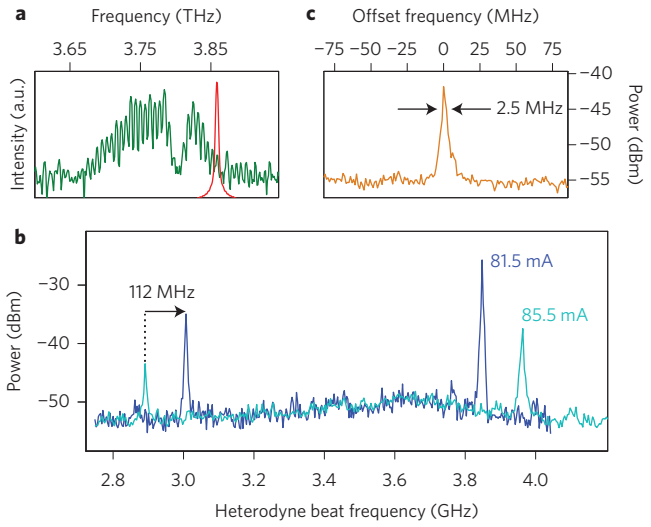

Figure 5 | Heterodyne beat note between single-mode laser and comb. **a**, Correlation spectrum of comb at 0.9 A (green) and spectrum of DFB laser (red). **b**, Heterodyne beating of free-running comb laser at 0.885 A with free-running DFB laser at various biases. The two lines correspond to beating between the two nearest comb lines and sum to the repetition rate of 6.8 GHz. The tuning coefficient of the DFB is 28 MHz mA^{-1}. **c**, Zoomed-in view of one of the lines, showing a convolved FWHM of 2.5 MHz. From this, we estimate that our comb lines are 1.8 MHz wide.

bias, we observe that the two lines move in opposite directions by the laser's tuning coefficient (28 MHz mA^{-1} in this case[33]). Even though the DFB laser is operating near the edge of the comb's bandwidth and only a few percent of the DFB's power can be coupled into the metal–metal waveguide, we are still able to measure beat notes with signal-to-noise ratios exceeding 10 dB. Figure 5c shows one of these beat notes over a smaller frequency span. Because the DFB's frequency and comb's offset frequency are both unstabilized, the measured full-width at half-maximum (FWHM) linewidth of 2.5 MHz represents a convolution between their respective lineshapes. Assuming they are identical Gaussians, we can infer an absolute comb linewidth of 1.8 MHz. Previous characterization of similar DFB lasers has measured free-running linewidths between 1 and 3 MHz (ref. 34), showing that our comb's offset frequency is as stable as a single-mode laser. Such linewidths are more than suitable for dual-comb spectroscopy at these wavelengths, due to the large ratio of the laser's repetition rate to its frequency.

In conclusion, we have demonstrated that THz QCLs can be used to generate high-power, broadband frequency combs. By applying dispersion compensation techniques from visible wavelengths to the THz QCL, we have shown that an arbitrary gain medium can be made to produce passive combs. Such combs cover a frequency range of almost 500 GHz with more than 70 lines at 3.5 THz and represent nearly an order of magnitude improvement over the ten modes obtained by active mode-locking[16]. The comb's bandwidth covers 14% of its centre frequency—the highest fractional bandwidth of integrated semiconductor frequency combs to date—suggesting that similar techniques can be used to improve Kerr-like combs at other wavelengths, including the mid-infrared. We have demonstrated SWIFT spectroscopy, a coherent detection scheme that can be used in combination with FTS to quantitatively measure the performance of such lasers and to measure the efficacy of comb formation. We have also demonstrated that, by utilizing intracavity mixing, these lasers can be used to compactly measure the frequency of single-mode lasers without the need for a high-speed terahertz detector or an external solid-state laser. To be truly useful for compact sensing applications, however, further development is still required. At present, the gain medium's double-peaked shape causes the laser's energy to be split across two lobes and limits its general applicability, as the region between the two lobes experiences too much loss and cannot be accessed without a high-dynamic range detector. In addition, the weak interaction between the two lobes leads to a complicated bias dependence of the comb's properties and reduces its robustness. Fortunately, both of these issues are straightforward to resolve, as continuing development of heterogeneous gain media[35] will lead to flatter, broader comb spectra. Once octave-spanning spectra can be achieved, it may even be possible to stabilize the comb's absolute frequency[36,37] without any additional components, because the intracavity mixing process we demonstrated should also be capable of generating f–$2f$ beating. Such combs could be used to form compact solid-state dual-comb spectrometers, which by utilizing intracavity mixing may even be able to operate without external detectors.

Methods

Terahertz time-domain spectroscopy. Dispersion and gain measurements were performed using a 775-μm-long, 30-μm-wide Fabry–Pérot QCL made from the same gain medium as the frequency comb devices, FL183S (wafer VB0481). Near-infrared pulses from a Ti:sapphire laser (80 fs, 25 mW) were shone into the facet of a biased laser, and the resulting terahertz pulses were used to characterize it. The first pulse that exits has passed through the waveguide once, whereas the second pulse has passed through three times. The amplitude ratio gives the gain, while the phase difference gives the dispersion. A silicon hyperhemispherical lens was attached to the output facet and electro-optic sampling[38] was used to sample the waveform, using a 300 μm [110] GaP wafer bonded to three 400 μm [100] GaP wafers.

Homodyne interferometry (SWIFT spectroscopy). Light from the lens-coupled THz QCL comb was collimated by an f/2 off-axis parabolic mirror (OAP), attenuated by a factor of 40 using a screen to prevent HEB saturation and passed through an optical chopper. It was then passed through a custom-built nitrogen-purged FTS that utilizes roof mirrors to minimize retroreflection into the QCL, and uses 1 mm of high-resistivity silicon as a beam splitter. Finally, light was focused onto the HEB using an f/3 OAP. The HEB was biased to 1 mV using a custom bias box and the current monitor was passed into a lock-in amplifier for the normal interferogram. The RF port of the HEB's bias-tee was amplified with a cryogenic low-noise amplifier (27 dB gain) and a room-temperature amplifier (31 dB gain). The RF signal was then downconverted and demodulated (Supplementary Fig. 2a) and the I and Q signals passed into lock-in amplifiers. All lock-ins used the same time constant of 1 ms, and the stage speeds used were 0.1 mm s^{-1} (Fig. 3) and 0.3 mm s^{-1} (Fig. 4). The FTS travel range was 10.75 cm, resulting in a resolution of 1.5 GHz.

Heterodyne beat-note measurement. For the heterodyne beating measurements of Fig. 5, a third-order DFB[39,40] was constructed using metal–metal waveguides fabricated from the same gain medium as the comb. It was 21 μm wide, 450 μm long and consisted of 15 periods of a corrugation that lased at 3.85 THz, with about a milliwatt of power. The DFB was operated in continuous-wave mode in a compact Stirling cryocooler at 47 K and its light was collimated using an f/3 OAP and focused onto the comb laser with an f/2 OAP. The RF beat notes were collected from the comb laser using a bias-tee and amplified with a low-noise amplifier providing 50 dB of gain. The resolution bandwidth for all heterodyne beat-note measurements was 3 MHz. The sweep times used in Fig. 5b,c were 31 ms and 51 ms, respectively.

Received 28 January 2014; accepted 28 March 2014; published online 11 May 2014

References

1. Udem, Th., Holzwarth, R. & Hänsch, T. W. Optical frequency metrology. *Nature* **416,** 233–237 (2002).
2. Mandon, J., Guelachvili, G. & Picqué, N. Fourier transform spectroscopy with a laser frequency comb. *Nature Photon.* **3,** 99–102 (2009).
3. Ferguson, B. & Zhang, X.-C. Materials for terahertz science and technology. *Nature Mater.* **1,** 26–33 (2002).
4. Shen, Y.-C. *et al.* Detection and identification of explosives using terahertz pulsed spectroscopic imaging. *Appl. Phys. Lett.* **86,** 241116 (2005).
5. Schmuttenmaer, C. A. Exploring dynamics in the far-infrared with terahertz spectroscopy. *Chem. Rev.* **104,** 1759–1780 (2004).
6. Köhler, R. *et al.* Terahertz semiconductor-heterostructure laser. *Nature* **417,** 156–159 (2002).
7. Brandstetter, M. *et al.* High power terahertz quantum cascade lasers with symmetric wafer bonded active regions. *Appl. Phys. Lett.* **103,** 171113 (2013).

8. Kourogi, M., Nakagawa, K. & Ohtsu, M. Wide-span optical frequency comb generator for accurate optical frequency difference measurement. *IEEE J. Quantum Electron.* **29,** 2693–2701 (1993).
9. Kippenberg, T. J., Holzwarth, R. & Diddams, S. A. Microresonator-based optical frequency combs. *Science* **332,** 555–559 (2011).
10. Yeh, K.-L., Hoffmann, M. C., Hebling, J. & Nelson, K. A. Generation of 10 μJ ultrashort terahertz pulses by optical rectification. *Appl. Phys. Lett.* **90,** 171121 (2007).
11. Pearson, J. C. *et al.* Demonstration of a room temperature 2.48–2.75 THz coherent spectroscopy source. *Rev. Sci. Instrum.* **82,** 093105 (2011).
12. Drouin, B. J., Maiwald, F. W. & Pearson, J. C. Application of cascaded frequency multiplication to molecular spectroscopy. *Rev. Sci. Instrum.* **76,** 093113 (2005).
13. Ippen, E. P. Principles of passive mode locking. *Appl. Phys. B* **58,** 159–170 (1994).
14. Wang, C. Y. *et al.* Coherent instabilities in a semiconductor laser with fast gain recovery. *Phys. Rev. A* **75,** 031802 (2007).
15. Wang, C. Y. *et al.* Mode-locked pulses from mid-infrared quantum cascade lasers. *Opt. Express* **17,** 12929–12943 (2009).
16. Barbieri, S. *et al.* Coherent sampling of active mode-locked terahertz quantum cascade lasers and frequency synthesis. *Nature Photon.* **5,** 306–313 (2011).
17. Hugi, A., Villares, G., Blaser, S., Liu, H. C. & Faist, J. Mid-infrared frequency comb based on a quantum cascade laser. *Nature* **492,** 229–233 (2012).
18. Keilmann, F., Gohle, C. & Holzwarth, R. Time-domain mid-infrared frequency-comb spectrometer. *Opt. Lett.* **29,** 1542–1544 (2004).
19. Bernhardt, B. *et al.* Cavity-enhanced dual-comb spectroscopy. *Nature Photon.* **4,** 55–57 (2010).
20. Lee, A. W. M., Kao, T.-Y., Burghoff, D., Hu, Q. & Reno, J. L. Terahertz tomography using quantum-cascade lasers. *Opt. Lett.* **37,** 217–219 (2012).
21. Kärtner, F. X. *et al.* Ultrabroadband double-chirped mirror pairs for generation of octave spectra. *J. Opt. Soc. Am. B* **18,** 882–885 (2001).
22. Kröll, J. *et al.* Phase-resolved measurements of stimulated emission in a laser. *Nature* **449,** 698–701 (2007).
23. Burghoff, D. *et al.* A terahertz pulse emitter monolithically integrated with a quantum cascade laser. *Appl. Phys. Lett.* **98,** 061112 (2011).
24. Martl, M. *et al.* Gain and losses in THz quantum cascade laser with metal–metal waveguide. *Opt. Express* **19,** 733–738 (2011).
25. Burghoff, D., Wang, C. W. I., Hu, Q. & Reno, J. L. Gain measurements of scattering-assisted terahertz quantum cascade lasers. *Appl. Phys. Lett.* **100,** 261111 (2012).
26. Lee, A. W. M. *et al.* High-power and high-temperature THz quantum-cascade lasers based on lens-coupled metal–metal waveguides. *Opt. Lett.* **32,** 2840–2842 (2007).
27. Kumar, S. & Hu, Q. Coherence of resonant-tunneling transport in terahertz quantum-cascade lasers. *Phys. Rev. B* **80,** 245316 (2009).
28. Gellie, P. *et al.* Injection-locking of terahertz quantum cascade lasers up to 35 GHz using RF amplitude modulation. *Opt. Express* **18,** 20799–20816 (2010).
29. Zhang, W. *et al.* Quantum noise in a terahertz hot electron bolometer mixer. *Appl. Phys. Lett.* **96,** 111113 (2010).
30. Baryshev, A. *et al.* Phase locking and spectral linewidth of a two-mode terahertz quantum cascade laser. *Appl. Phys. Lett.* **89,** 031115 (2006).
31. Gordon, A. *et al.* Multimode regimes in quantum cascade lasers: from coherent instabilities to spatial hole burning. *Phys. Rev. A* **77,** 053804 (2008).
32. Dhillon, S. S. *et al.* Terahertz transfer onto a telecom optical carrier. *Nature Photon.* **1,** 411–415 (2007).
33. Hayton, D. J. *et al.* Phase locking of a 3.4 THz third-order distributed feedback quantum cascade laser using a room-temperature superlattice harmonic mixer. *Appl. Phys. Lett.* **103,** 051115 (2013).
34. Ren, Y. *et al.* Frequency locking of single-mode 3.5-THz quantum cascade lasers using a gas cell. *Appl. Phys. Lett.* **100,** 041111 (2012).
35. Turčinková, D. *et al.* Ultra-broadband heterogeneous quantum cascade laser emitting from 2.2 to 3.2 THz. *Appl. Phys. Lett.* **99,** 191104 (2011).
36. Vitiello, M. S. *et al.* Quantum-limited frequency fluctuations in a terahertz laser. *Nature Photon.* **6,** 525–528 (2012).
37. Consolino, L. *et al.* Phase-locking to a free-space terahertz comb for metrological-grade terahertz lasers. *Nature Commun.* **3,** 1040 (2012).
38. Wu, Q. & Zhang, X.-C. Free-space electro-optic sampling of terahertz beams. *Appl. Phys. Lett.* **67,** 3523–3525 (1995).
39. Amanti, M. I., Fischer, M., Scalari, G., Beck, M. & Faist, J. Low-divergence single-mode terahertz quantum cascade laser. *Nature Photon.* **3,** 586–590 (2009).
40. Kao, T.-Y., Hu, Q. & Reno, J. L. Perfectly phase-matched third-order distributed feedback terahertz quantum-cascade lasers. *Opt. Lett.* **37,** 2070–2072 (2012).

Acknowledgements

The work at MIT was supported by NASA and the NSF. The work in the Netherlands was supported by NWO, NATO SFP and RadioNet. This work was performed, in part, at the Center for Integrated Nanotechnologies, a US Department of Energy, Office of Basic Energy Sciences user facility. Sandia National Laboratories is a multi-programme laboratory managed and operated by Sandia Corporation, a wholly owned subsidiary of Lockheed Martin Corporation, for the US Department of Energy's National Nuclear Security Administration (contract no. DE-AC04-94AL85000). The authors thank D. Levonian for his help in setting up the FTIR.

Author contributions

D.B. conceived the strategy, designed the devices, performed the measurements and completed the analysis. D.B. and N.H. performed electromagnetic simulations. T.-Y.K., N.H. and C.W.I.C. fabricated the devices. D.B., X.C. and Y.Y. performed the heterodyne beat-note measurements. D.J.H. and J.-R.G. provided the hot electron bolometer mixer. J.L.R. provided the material growth. All work was performed under the supervision of Q.H.

Additional information

Supplementary information is available in the online version of the paper. Reprints and permissions information is available online at www.nature.com/reprints. Correspondence and requests for materials should be addressed to D.B.

Competing financial interests

The authors declare no competing financial interests.

nature photonics

SUPPLEMENTARY INFORMATION

DOI: 10.1038/NPHOTON.2014.85

Terahertz laser frequency combs Supplementary information

David Burghoff[1*], Tsung-Yu Kao[1], Ningren Han[1], Chun Wang Ivan Chan[1], Xiaowei Cai[1], Yang Yang[1], Darren J. Hayton[2], Jian-Rong Gao[2,3], John L. Reno[4], and Qing Hu[1]

Design of dispersion-compensating corrugations

In order to design the corrugations used for dispersion compensation, one-dimensional simulations were first performed that captured the essential behavior of the structures. The key parameters, shown in Supp. Fig. 1a, are the corrugation length, its start period, its stop period, how quickly its amplitude tapers on (e.g., linearly), and its largest amplitude. To first order, the start and stop periods determine the maximum and minimum frequencies at which dispersion is compensated, while the corrugation length determines the amount of compensation. How quickly the amplitude tapers on determines how strong ripples in the final group delay are, while the largest amplitude determines the bandwidth over which the group delay can remain linear. Full-wave finite element (FEM) simulations were then performed to verify design efficacy, and the compensators' group delay versus frequency were plotted. Supp. Fig. 1b shows two such designs. Even though they differ in their compensation by nearly an order of magnitude, linearity is maintained over the whole design range of 3 THz to 4 THz. Though sidewall-based corrugations were used here, any perturbation that introduces a refractive index change into the waveguide (such as an etched trench or a region of removed metal) can also be used to construct compensators.

To demonstrate the necessity of proper compensation, we plot in Supp. Fig. 1c the RF power generated by three QCLs differing in their dispersion compensation by steps of only 6.7%. When the compensation is detuned from the correct compensation of 1.25 ps^2/mm (+13.3%) even slightly, no RF beatnote is generated and no comb is formed. (At high biases in the devices' negative differential resistance regimes, RF radiation spanning several GHz can be generated, though this is merely due to electrical instability.) Indeed, this highly sensitive dependence on proper dispersion compensation explains why no spontaneous broadband comb formation has ever been reported in THz QCLs to date.

Setup for frequency locking and SWIFTS

Supplementary Figure 2a shows both the setup used for stabilizing the QCL's repetition rate against mechanical vibration of the cryocooler and for homodyne interferometry (SWIFTS). For repetition rate stabilization, the free-running beatnote emanating from the QCL is first observed on a spectrum analyzer, which is typically near 6.8 GHz. An external frequency synthesizer (HP 8673E) is tuned to be 10 MHz away from the free-running signal. The QCL beatnote is then downconverted twice, first to 10 MHz and then to DC, and is used as the error signal for a PI controller. The output of the PI controller is added to the QCL bias with a 3 kΩ resistor, and since the QCL's bias affects the refractive index and

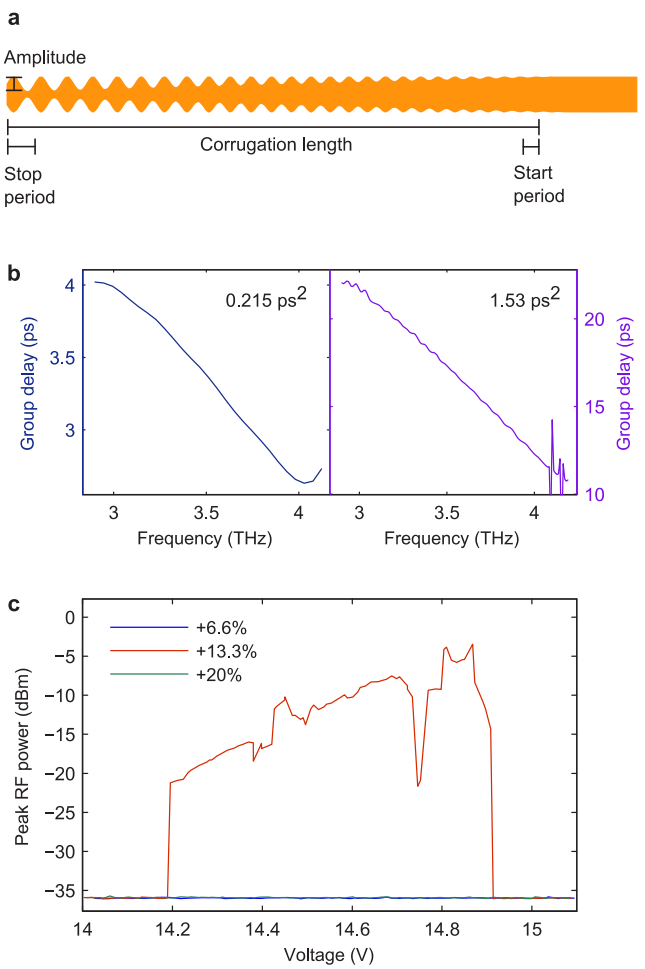

Supplementary Figure 1 | Dispersion compensation design. a, Schematic showing the key parameters of the dispersion compensators. **b,** Simulated group delay versus frequency plots for the smallest and the largest compensators developed, respectively. A linear response compensates for second-order dispersion. **c,** RF beatnote emanating from three QCLs with compensations of 1.17 ps^2/mm (+6.6%), 1.25 ps^2/mm (+13.3%), and 1.32 ps^2/mm (+20%).

[1]Department of Electrical Engineering and Computer Science, Research Laboratory of Electronics, Massachusetts Institute of Technology, Cambridge, Massachusetts 02139, USA. [2]SRON Netherlands Institute for Space Research, 9747 AD, Groningen, Netherlands [3]Kavli Institute of NanoScience, Delft University of Technology, Lorentzweg 1, 2628 CJ Delft, The Netherlands [4]Center for Integrated Nanotechnology, Sandia National Laboratories, Albuquerque, NM 87123 *e-mail: burghoff@mit.edu

DOI: 10.1038/NPHOTON.2014.85

therefore repetition rate, this locks the QCL's repetition rate to the frequency of the synthesizer plus 10 MHz. Note that as we are not performing injection locking, the added current only has frequency components up to about 100 kHz, and has an amplitude of less than a milliamp (much smaller than the DC bias of ~1 A). Also note that while the HEB has alternatively been used to perform repetition rate stabilization, doing so prevents it from being used in homodyne interferometry. Supp. Figure 2b shows the effect of locking the repetition rate on the beatnote, as measured on the HEB. The inset shows an RF spectrum of an unstabilized laser. Even though the signal-to-noise ratio of the measurement is quite high, 45 dB, its center frequency fluctuates over long time scales as a result of the laser's unstable environment, giving an apparent linewidth of almost 100 kHz. In contrast, when the beatnote is locked to an external local oscillator, its linewidth can be reduced substantially, to only a few Hz or less.

During SWIFT measurements, the signal from the HEB is amplified and downconverted by the reference synthesizer (near 6.8 GHz) to 10 MHz. It is then demodulated using a 10 MHz I/Q demodulator, producing the two components of the RF signal, and measured with a pair of lock-in amplifiers. (The quasi-DC component of the HEB signal is also measured.) All three lock-ins use the same time constant, amplitude, and phase settings, and as the Michelson interferometer's stage is scanned, their signals are simultaneously recorded.

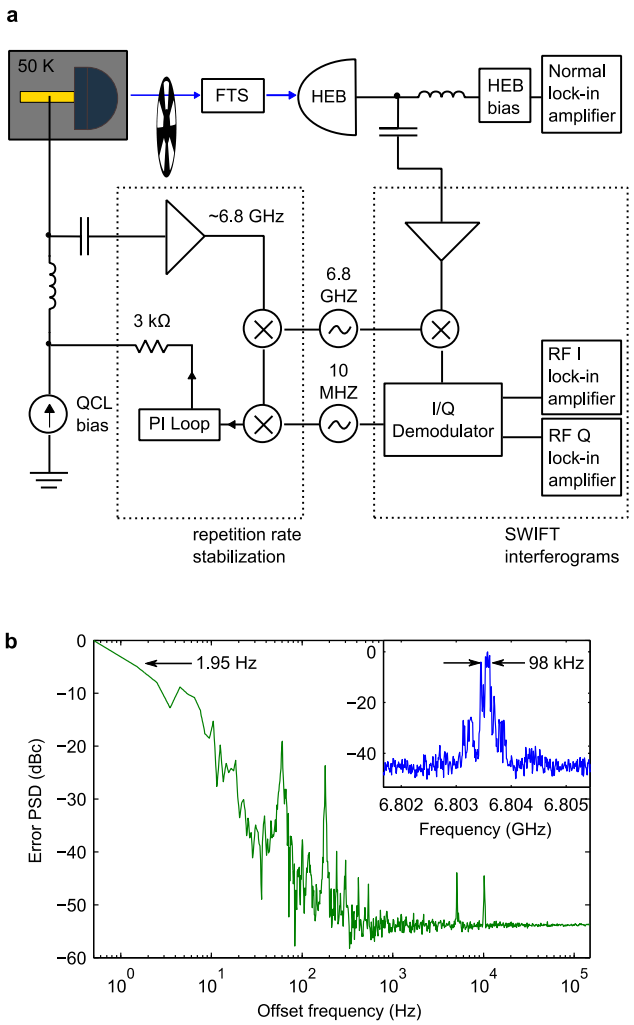

Supplementary Figure 2 | Locking the repetition rate and performing SWIFTS. a, Block diagram showing the repetition rate stabilization and the homodyne interferogram measurement. **b,** Phase error generated by mixing the locked HEB beatnote with the local oscillator. The FWHM linewidth is 1.95 Hz, and the only major sidebands are 60 Hz harmonics likely arising from clock error. Inset: Unstabilized HEB beatnote measured on an RF spectrum analyzer. Because the beatnote is dominated by long-term frequency fluctuations, a large video bandwidth of 3 MHz was used. The FWHM linewidth is 98 kHz.

SWIFT spectroscopy analysis

If E(t) is the electric field produced by a light source, the instantaneous intensity signal impinging on a detector after passing through a Michelson interferometer can be expressed as

$$S(t) = \frac{1}{2}(E(t) + E(t-\tau))^2$$

where S(t) is the instantaneous intensity, E(t) is the electric field, and τ is the stage delay. If the electric field is expanded in terms of its Fourier components using the convention that

$$E(t) = \sum_{\omega} E(\omega) e^{i\omega t}$$

then the usual interferogram measured at DC can be expressed as the zero-frequency component of S(t), or

$$S_0(\tau) = \left\langle (E(t) + E(t-\tau))^2 \right\rangle = \sum_{\omega>0} |E(\omega)|^2 e^{i\omega\tau} + |E(\omega)|^2 + c.c.$$

To measure a SWIFT spectrum, the signal is instead mixed with a local oscillator, defined here using the convention that $V(t)=2\cos(\Delta\omega t+\phi)$ (where $\Delta\omega$ is its frequency and ϕ is its phase). One can then show that the resulting signal is

$$S_{\Delta\omega,\phi}(\tau) = \sum_{\omega>0} \left[E^*(\omega)E(\omega-\Delta\omega)e^{i\phi} + E^*(\omega)E(\omega+\Delta\omega)e^{-i\phi} \right] e^{i\omega\tau} + \left[E^*(\omega)E(\omega-\Delta\omega)e^{i\phi} \right](1+e^{i\Delta\omega\tau}) + c.c.$$

Some comparisons between the homodyne and normal interferograms are in order. Both of course contain terms oscillating at the frequencies the laser produces, and both contain constant terms as well. Interestingly enough, the homodyne interferogram also contains a term oscillating at $e^{i\Delta\omega\tau}$, the frequency of the laser's repetition rate. This term is clearly visible in the zoomed-out interferograms of Figure 3a. The constant term corresponds to the non-interferometric contribution of the interferometer's fixed arm, while the term oscillating at $\Delta\omega$ corresponds to the non-interferometric contribution of the interferometer's variable arm. In addition, while the components of the normal interferogram are strictly positive (and have zero phase), the homodyne interferograms obey no such constraint. As a result, they can be asymmetric about the zero-path delay.

Since the global group delay is arbitrary, without loss of generality one can assume that $\phi=0$ for the in-phase signal and $\phi=-\pi/2$ for the in-quadrature signal. The positive frequency components are then found to be the following:

$$S_I(\omega) = E^*(\omega)E(\omega-\Delta\omega) + E^*(\omega)E(\omega+\Delta\omega)$$
$$S_Q(\omega) = i(-E^*(\omega)E(\omega-\Delta\omega) + E^*(\omega)E(\omega+\Delta\omega))$$

This in turn implies that

$$E^*(\omega)E(\omega\pm\Delta\omega) = \frac{1}{2}(S_I(\omega) \mp iS_Q(\omega)) \equiv X_{\pm}(\omega)$$

as stated in the text. One way to validate this approach is to note that $X_+(\omega)$ and $X_-(\omega)$ would ideally not be independent of each other; in fact they should be trivially related by $X_-(\omega+\Delta\omega)=X_+^*(\omega)$. By plotting $X_+(\omega)$'s and $X_-(\omega)$'s magnitudes and shifting one of them by $\Delta\omega$, we can see if this is the case. Supp. Figure 3 shows the result of this process. The top panel shows the Fourier transforms of the raw I and Q interferograms, which differ quite a bit since there's no reason for them to be the same. In contrast, the computed correlations in the bottom panel would be identical if not for the presence of noise. In fact, they can even be averaged to marginally improve the signal-to-noise ratio of the measurement.

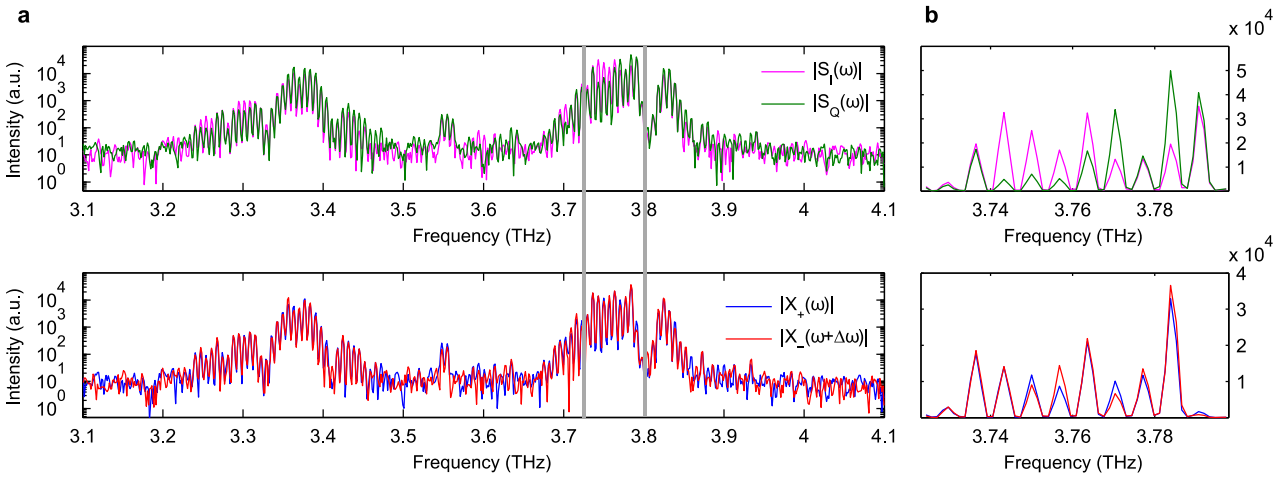

Supplementary Figure 3 | Consistency of SWIFT data. a, Top panel: raw Fourier transforms of the I and Q interferograms of the data in Fig. 3a. Bottom panel: calculated SWIFT correlation magnitudes, with X. shifted by the repetition rate of the laser. **b,** The zoomed-in region is plotted on a linear scale.

Finally, note that the phase of the correlation functions represents the phase difference between adjacent comb lines, $\Delta\varphi$. In principle, this makes SWIFTS a rival to full-field pulse characterization techniques like FROG[1] and SPIDER[2]. In practice, however, this is difficult since only phase differences are measured and therefore requires a cumulative sum to get the actual phases. The resulting inference is highly subject to noise. However, since group delay can be estimated as $\tau_g \approx \Delta\varphi/\Delta\omega$, this means that SWIFTS can still be used to determine the frequency-dependent group delay (modulo the cavity round-trip time).

References

1. Trebino, R. et al. Measuring ultrashort laser pulses in the time-frequency domain using frequency-resolved optical gating. Review of Scientific Instruments 68, 3277–3295 (1997).
2. Iaconis, C. & Walmsley, I. A. Spectral phase interferometry for direct electric-field reconstruction of ultrashort optical pulses. Opt. Lett. 23, 792–794 (1998).